ADVANCES IN ATMOSPHERIC SCIENCES, VOL. 35, FEBRUARY 2018, 158–168

• **Original Paper** •

# Climatology of Cloud-base Height from Long-term Radiosonde Measurements in China

Yong ZHANG[1], Lejian ZHANG[1], Jianping GUO[*2], Jinming FENG[3], Lijuan CAO[4], Yang WANG[5], Qing ZHOU[1], Liangxu LI[1], Bai LI[1], Hui XU[2], Lin LIU[2], Ning AN[5], and Huan LIU[2]

[1]*Meteorological Observation Center, China Meteorological Administration, Beijing* 100081*, China*
[2]*State Key Laboratory of Severe Weather, Chinese Academy of Meteorological Sciences, Beijing* 100081*, China*
[3]*Key Laboratory of Regional Climate-Environment for Temperate East Asia, Institute of Atmospheric Physics, Chinese Academy of Sciences, Beijing* 100029*, China*
[4]*National Meteorological Information Center, China Meteorological Administration, Beijing* 100081*, China*
[5]*College of Global Change and Earth System Science, Beijing Normal University, Beijing* 100875*, China*

(Received 15 April 2017; revised 7 September 2017; accepted 9 October 2017)

ABSTRACT

Clouds are critical to the global radiation budget and hydrological cycle, but knowledge is still poor concerning the observed climatology of cloud-base height (CBH) in China. Based on fine-resolution sounding observations from the China Radiosonde Network (CRN), the method used to estimate CBH was modified, and uncertainty analyses indicated that the CBH is good enough. The accuracy of CBH estimation is verified by the comparison between the sounding-derived CBHs and those estimated from the micro-pulse lidar and millimeter-wave cloud radar. As such, the CBH climatology was compiled for the period 2006–16. Overall, the CBH exhibits large geographic variability across China, at both 0800 Local Standard Time (LST) and 2000 LST, irrespective of season. In addition, the summertime cloud base tends to be elevated to higher altitudes in dry regions [i.e., Inner Mongolia and the North China Plain (NCP)]. By comparison, the Tibetan Plateau (TP), Pearl River Delta (PRD) and Sichuan Basin (SCB) have relatively low CBHs (< 2.4 km above ground level). In terms of seasonality, the CBH reaches its maximum in summer and minimum in winter. A low cloud base tends to occur frequently (> 70%) over the TP, PRD and SCB. In contrast, at most sites over the Yangtze River Delta (YRD) and the NCP, about half the cloud belongs to the high-cloud category. The CBH does not exhibit marked diurnal variation in summer, throughout all CRN sites, probably due to the persistent cloud coverage caused by the East Asia Summer Monsson. To the best of our knowledge, this is the first CBH climatology produced from sounding measurements in China, and provides a useful reference for obtaining observational cloud base information.

**Key words**: cloud base height, radiosonde, relative humidity, China, climatology

**Citation**: Zhang, Y., and Coauthors, 2018: Climatology of cloud-base height from long-term radiosonde measurements in China. *Adv. Atmos. Sci.*, **35**(2), 158–168, https://doi.org/10.1007/s00376-017-7096-0.

## 1. Introduction

Cloud plays a significant role in the Earth's energy budget by reflecting and absorbing incoming solar radiation and reducing outgoing thermal radiation (Stephens et al., 2012; Zhou et al., 2016). The impacts of cloud on the radiation balance of the Earth–atmosphere system depend not only on the vertical structure and distribution of the cloud but also on its base and top heights and optical properties (Wild, 2012; Zhang et al., 2017a). Cloud radiative forcings, especially those induced by aerosol–cloud interaction (Wang et al., 2015; Guo et al., 2016a, 2017), further contribute to uncertainties in weather forecasting and climate prediction (Li et al., 2016). Cloud properties have changed and will continue to change in a warming climate, including changes in cloud height, cloud cover, and morphology (Eastman and Warren, 2013). For decades, both observations and models have been extensively used to elucidate the characteristics of cloud and their corresponding changes on the daily, seasonal and yearly time scales (Klein and Hartmann, 1993; Baker and Peter, 2008; Clement et al., 2009; Davies and Molloy, 2012; Shonk et al., 2012; Zelinka et al., 2013; Myers and Norris, 2015; Miao et al., 2017).

The properties of cloud are generally associated with cloud types, and the climate effects caused by various cloud types differ greatly; in some circumstances they are even totally opposite. For instance, high cloud has a warming effect

* Corresponding author: Jianping GUO
Email: jpguocams@gmail.com

on the surface, as opposed to the cooling effect of low-level clouds (IPCC, 2013). Unfortunately, cloud profiles are poorly understood at present and remain a primary source of uncertainty in global weather and climate studies (Stephens, 2005).

The retrieval of cloud profiles relies primarily on satellite- (e.g., Minnis and Harrison, 1984; Morel and Senesi, 2002) and surface-based observations (e.g., Dong et al., 2006). The advent of spaceborne active cloud radar (e.g., CloudSat) has allowed for a better portrayal of cloud vertical structure on both regional and global scales, making it one of the most popular data sources for cloud studies (Stephens et al., 2002; Sassen and Wang, 2008; Naud et al., 2010; Evan and Norris, 2012; Chen et al., 2016).

Cloud-base height (CBH) is an important cloud macrophysical parameter, strongly affecting the energy exchanges between the cloud layer and the ground surface (Wild, 2012). Using the cloud profiles and CBH data determined from the active-sounding measurements of CloudSat and CALIPSO has helped resolve the long-standing debate over the underestimation of thermal back-radiation, which has been updated from the previous estimate of 324 W $m^{-2}$ (Kiehl and Trenberth, 1997) to around 345–350 W $m^{-2}$ (Kato et al., 2011; Stephens et al., 2012). However, thin clouds cannot be accurately identified by the cloud profiling radar onboard CloudSat (Marchand et al., 2008). A recent study indicated that large uncertainties exist in the CBH from CloudSat–CALIPSO data, based on comparison with ground-based active remote sensing of cloud (Zhang et al., 2017b).

In comparison to satellite measurements, ground-based cloud observations based on instruments such as cloud radars, lidars (e.g., Borg et al., 2011) and ceilometers (e.g., Martucci et al., 2010; Costa-Surós et al., 2009), can provide CBH measurements with higher accuracy and continuous temporal coverage (Sharma et al., 2016). In North America, an automated observation system employs ceilometers to observe cloud. However, these ceilometers observe cloud at a cutoff range, generally lower than 4 km (Dai et al., 2006). In other parts of the world, these instruments are generally deployed at very few locations. Fortunately, radiosondes can also penetrate cloud layers to provide in-situ measurements such as temperature, relative humidity and pressure, which are fundamental to estimating the profiles of atmospheric and cloud properties (Poore et al., 1995; Zhang et al., 2010). More importantly, operational radiosonde networks make it possible to retrieve the CBH over a large scale. For example, Wang and Rossow (1995) successfully obtained the cloud vertical structure based on relative humidity (RH) sounding data alone, and Chernykh et al. (2001) analyzed worldwide long-term cloud-base and -top height trends based on RH and temperature sounding data.

Warren et al. (1986, 1988) produced a database from surface land stations and ship measurements and compiled a climatology of CBH over land and ocean by focusing on different cloud types (Warren et al., 2007; Eastman et al., 2011; Eastman and Warren, 2014). Sun et al. (2007) comprehensively analyzed the temporal trend of cloud-top heights and frequencies over the United States since the early 1950s, based mainly on human observations at weather stations. An et al. (2017) interpreted the diurnal, seasonal and interannual variability of the CBH over the contiguous United States based on an automated surface observing system.

However, notwithstanding a few CBH studies (e.g., Zhang et al., 2010) that were limited to a specific region of interest in China, no attempt (to the best of our knowledge) has been made to examine the climatology of CBH across China from long-term sounding observations from the China Radiosonde Network (CRN; Guo et al., 2016b). Accordingly, the main goals of the present study were to estimate the CBH with a robust method, and then elucidate the spatial and temporal characteristics of the CBH across China based on long-term soundings from the CRN. The remainder of the paper is organized as follows: Section 2 describes the data and the methods employed in this study. The uncertainty of the CBH estimation method is analyzed and discussed in section 3, followed in the same section by an analysis of the climatology, diurnal variation and seasonal differences of the CBH across China. The main conclusions are summarized in section 4.

## 2. Data and methods

### 2.1. *Sounding data*

The operational CRN consists of 120 sites equipped with L-band sounding systems, including GFE (L) 1 secondary wind radar and GTS1 digital electronic radiosondes (Guo et al., 2016b). The new-generation GTS1 digital radiosonde takes measurements of temperature, pressure, RH, wind speed, and wind direction twice a day [at 0800 Local Standard Time (LST, UTC+8) and 2000 LST], with a sampling frequency of once every 1.2 seconds. The vertical resolution varies from site to site, and from sounding to sounding at the same radiosonde site. A previous intercomparison of GTS1 against Vaisala RS80 indicated that they are in good agreement in terms of their profile measurements in the troposphere, despite a large bias in the upper atmospheric levels (Bian et al., 2011).

The setup of CRN dates back to 2002 when the China Meteorological Administration decided to upgrade existing radiosonde instruments; however, the GTS1 radiosonde at 14 sites only officially came into operation in 2006, as illustrated in Fig. 1. The L-band sounding systems with GTS1 radiosondes began to be widely deployed in 2007 across China, and had gradually expanded to 120 operational radiosonde stations by 2011. As such, each site of the CRN with GTS1 radiosonde data differs in their period of coverage (Fig. 1b). Overall, roughly 60% (97%) of radiosonde sites have more than 10 (6) years of L-band sounding data, which provides an even distribution across China and sufficient samples to characterize the climatology of the CBH from sounding data.

Therefore, the sounding data collected from the CRN during the period 1 December 2006 to 31 December 2016 were used to estimate the CBH across China. In summer (June–July–August), two additional soundings were launched (at 0200 LST and 1400 LST) to improve the predictability of

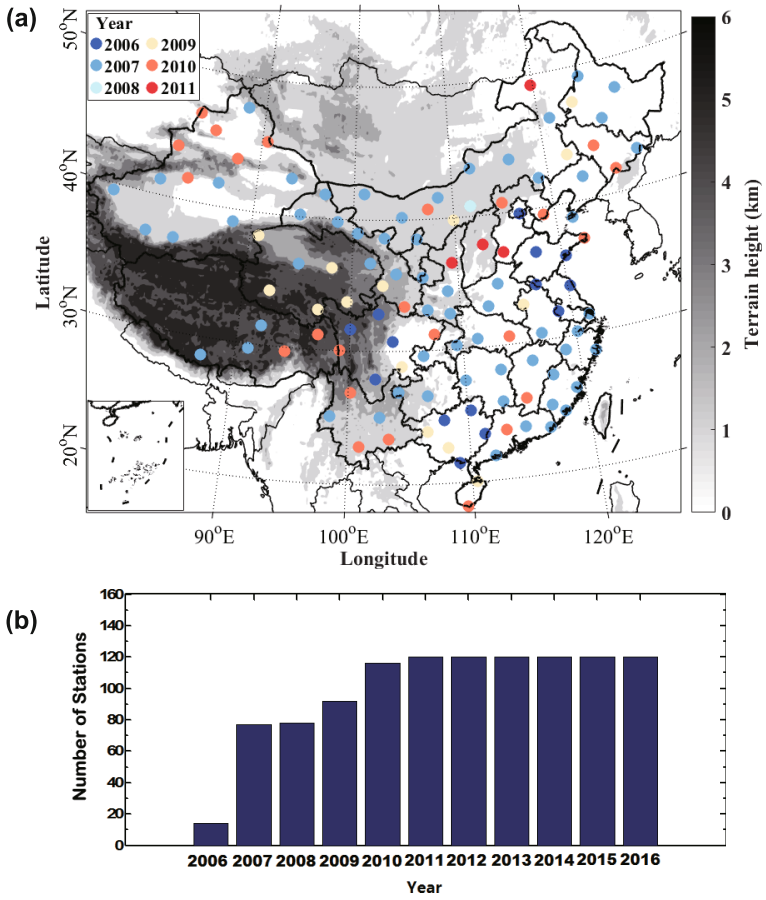


**Fig. 1.** (a) Spatial distribution of 120 sounding sites (colored circles) of the CMA over China. The different colors correspond to the year when the next-generation L-band radiosonde was first launched operationally. (b) Time series of the number of stations in the sounding sites dataset over China. The number of stations increased sharply in 2007, and reached 120 in 2011.

high-impact weather at selected sites of the CRN, depending on the locations of large-scale synoptic weather systems. In this way, we in total made use of 421 729 profiles across China, including 1979 profiles at 0200 LST, 208 445 profiles at 0800 LST, 9726 profiles at 1400 LST, and 201 579 profiles at 2000 LST.

### 2.2. *Methods*

Cloud generally forms at an RH of about 100%. It is, however, rarely observed in radiosonde observations for the reasons listed in Wang and Rossow (1995). In particular, the thermal lag tends to result in lower-than-normal RH values by about 3%, which is mainly caused by the temperature in the hygristor element being roughly 1°C above the ambient temperature as the radiosonde passes through the cloud layer (Garand et al., 1992). Regarding the hygristor inside the GTS1 of the CRN, the abovementioned thermal lag is too serious to be used to detect the cloud top (Bian et al., 2011). This is why the cloud top height was not investigated in this study.

In our analysis, the method proposed by Wang and Rossow (1995) was modified to better detect the cloud base, given the high temporal vertical resolution (1.2 s). First, the soundings under rainy conditions (rainfall amount > 0.1 mm) were excluded from the cloud-base detection. On average, 6.49% of all soundings witnessed valid precipitating events for all of the sounding hours during the period 2006–16 [Fig. S1 in electronic supplementary material (ESM)]. Therefore, the treatment of rainy sounding at missing value is reasonable. Then, the cloud base was determined by taking the following three steps: (1) the base of the lowest moist layer was determined as the average altitude where the minimum RH greater than 84% reached for at least four consecutive valid measurements; (2) an at least 3% jump in the RH could be seen from the adjacent lower level; and (3) the minimum CBH was set to 600 m above ground level (AGL) to avoid the noise caused by drizzle or rainfall below the cloud. In this way, RH profiles for all valid soundings were examined from 600 m AGL to the top to determine cloud bases.

To understand the frequency distribution of cloud with various CBH, the sounding-derived CBH retrievals were grouped into three height intervals: 0.6–2 km; 2–3.6 km; and above 3.6 km, with the 0.6–2-km category representing low cloud (Sun et al., 2007). Due to the spatial inhomogeneity,

all sites were interpolated onto a regular $5° \times 5°$ grid. Then, the CBH for each grid was calculated by simply averaging the available site data within the grid. In this way, any potential biases resulting from the spatial inhomogeneity of the radiosonde sites was minimized (Fig. 1a).

## 3. Results and discussion

### 3.1. *Uncertainty analysis*

The estimated CBH depends on the RH threshold values, which inevitably induces uncertainty in the CBH climatology. Uncertainty analysis, therefore, is imperative, and this is achieved by investigating the magnitude of changes in the CBH due to the selection of various critical RH thresholds.

Accordingly, scatterplots were produced that compare the CBH calculated using 84% and 83% as the critical RH versus those calculated using 84% and 85%. As expected, Figs. 2a and b show that the CBH based on RH = 85% (83%) is typically higher (lower) than that based on RH = 84%. However, the CBHs calculated using various RH thresholds are significantly correlated ($R = 0.987$). Figures 2c and d illustrate the absolute and relative uncertainties, respectively, as a function of CBH (RH = 84%). Most of the 50th and 75th percentile values of the absolute uncertainties are < 0.02 km and < 0.03 km, respectively; and the 50th and 75th percentile values of the corresponding relative uncertainties are both < 10% for CBH (RH = 84%) > 2 km, and < 20% for CBH (RH = 84%) within 1–2 km. In this sense, the uncertainty induced by the selection of the RH threshold is negligible.

But what about the accuracy of the CBH estimated from the chosen RH threshold? Based on a field campaign carried out by our group last summer in Xingtai (37.05°N, 114.48°E), Hebei Province, China, we took the CBH retrievals for May 2016 from the micro-pulse lidar (MPL) and millimeter-wave cloud radar (MMCR) implemented at Xingtai and compared them with the estimated CBHs from the radiosonde data. Figure S2 shows a comparison between the CBHs retrieved from MPL and MMCR and those from the radiosonde data on 25 May 2016. It can be seen that the difference in the CBH between the two data sources is quite small during the daytime, and in both cases the sky turns overcast after 2000 LST, suggesting a dominance of stratus cloud. Therefore, the CBH detected by radiosonde is comparable to that derived from the MPL under this condition. More specifically, the CBH from MPL is 5156 m when aver-

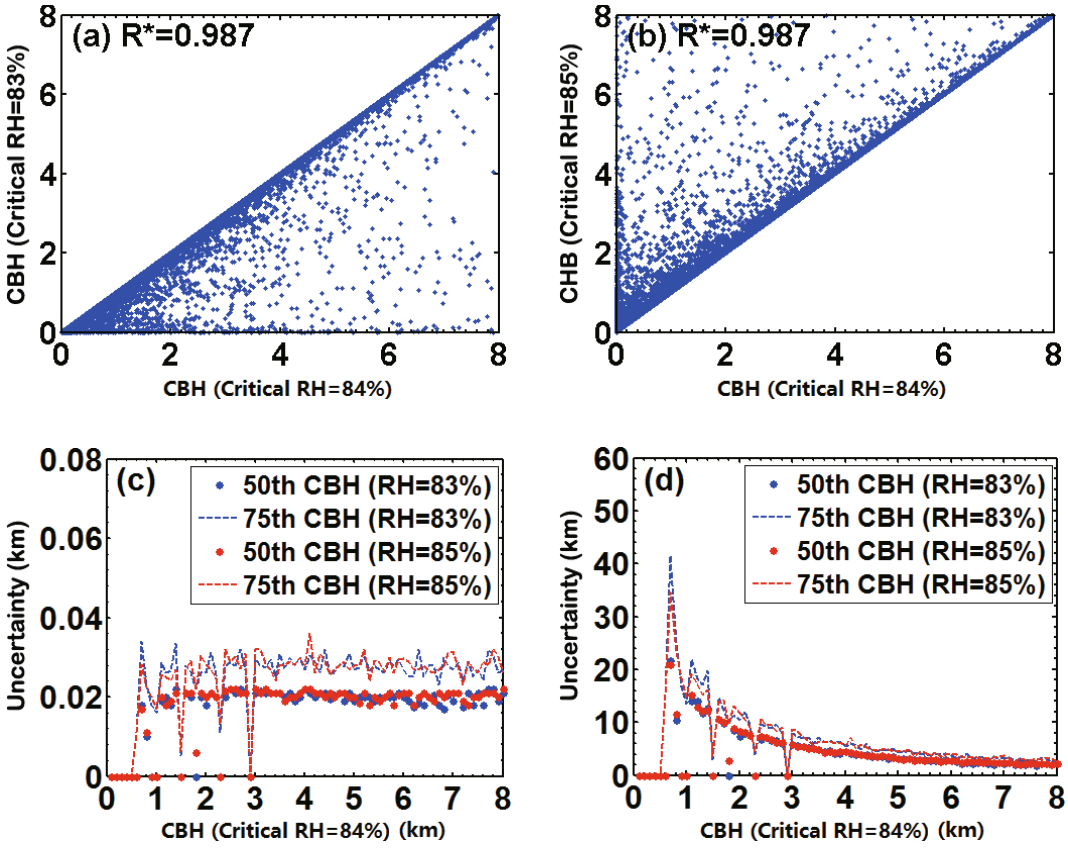


**Fig. 2.** Scatterplots showing CBH computed using (a) 84% and 83% and (b) 84% and 85% as the critical RH, both of which are based on 39 1552 soundings across China in summer during the period 2006–16. (c, d) The 50th and 75th percentile values of (c) absolute uncertainty and (d) relative uncertainty using 83% and 85% as the critical RH. The correlation coefficients ($R$) are given in the top panels, where an asterisk indicates the value is statistically significant ($p < 0.05$).

aged over the three minutes centered on the minute when the radiosonde detects the CBH, with a value of 4950 m. Therefore, the CBH results are in good agreement. Other cases throughout the field campaign at Xingtai from 15 May to 15 June 2016 were also examined (Fig. S3), the results of which verify that the CBH retrievals from MPL and radiosonde observations are consistent ($R = 0.998$).

### 3.2. *Geographic distribution and seasonality of CBH in China*

Figure 3 presents the geographic distribution of CBH derived from the 0800 LST radiosonde observations for the whole period from 2006 to 2016. Clearly, the CBH at 0800 LST does not exhibit strong latitudinal dependence. However, some strong spatial and seasonal variation stands out. On average, the CBH reaches its peak ($2.99 \pm 1.2$ km) in summer, followed by spring and fall, whereas the lowest CBH ($2.38 \pm 1.1$ km) is observed in winter. The strong contrast in CBH between summer and winter could be caused by the discrepancy in solar radiation reaching the surface. In addition, the lowest mean CBH found in winter is likely associated with the lowest temperature, which makes it easy for water vapor to condense or coalesce/collide to form cloud droplets under upward motion conditions, leading to a low cloud-top height.

Spatially, most sites in southwestern China, including the Tibetan Plateau (TP), Pearl River Delta (PRD) and Sichuan Basin (SCB), have a relatively low CBH (< 2.4 km AGL). Most sites in the Yangtze River Delta (YRD) and North China Plain (NCP) have a CBH greater than 3.6 km AGL in spring and summer, which is on average 0.6 km lower than that in fall and winter. In Northeast China, the summertime cloud can form at altitudes greater than 3.0 km—higher than the cloud in spring, fall and winter. Likewise, a peak in CBH can be seen in Inner Mongolia in summer, which is generally higher than 3.0 km AGL.

Similar to 0800 LST, the spatial variation of CBH at 2000 LST also does not exhibit distinct latitudinal dependence. Moreover, the spatial distributions of the 2000 LST CBH bear resemblance to those of the 0800 LST CBH, and the magnitude of the mean CBH in the four seasons changes little (Fig. 4). In terms of CBH seasonality, the springtime mean CBH is 2.86 km, which is slightly lower than that in summertime (2.92 km), and most radiosonde sites in winter have the lowest CBH. More specifically, the PRD has the lowest CBH in winter, and the CBH in NCP is highest in spring. The CBH diurnal and seasonal features in China are generally consistent with those obtained in the contiguous United States (An et al., 2017), which means that the geographic distribution of CBH in different seasons and at different times of the day have similar patterns.

### 3.3. *Frequency distribution of CBH*

Figure 5 shows the spatial distributions of CBH frequency for cloud bases within various altitudes at 0800 LST and 2000 LST during the period 2006–16. One striking feature is that the TP, PRD, and SCB are characterized by a high frequency (> 70%) of low cloud base (0.6 km < CBH < 2.0 km), sug-

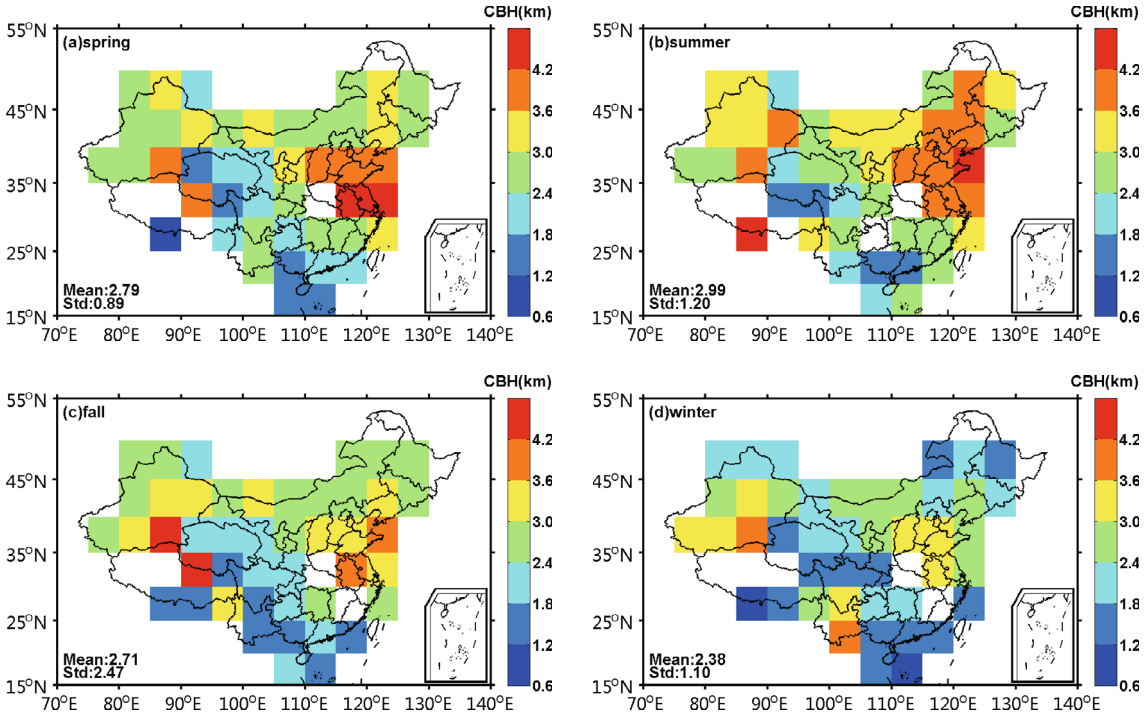


**Fig. 3.** Spatial distribution of CBH (color shaded) for each $5^\circ \times 5^\circ$ grid across China at 0800 LST in (a) spring, (b) summer, (c) fall, and (d) winter, for the period 2006–16. Note that CBH for each $5^\circ \times 5^\circ$ grid is calculated as the averaged CBH over all radiosonde sites within each grid.

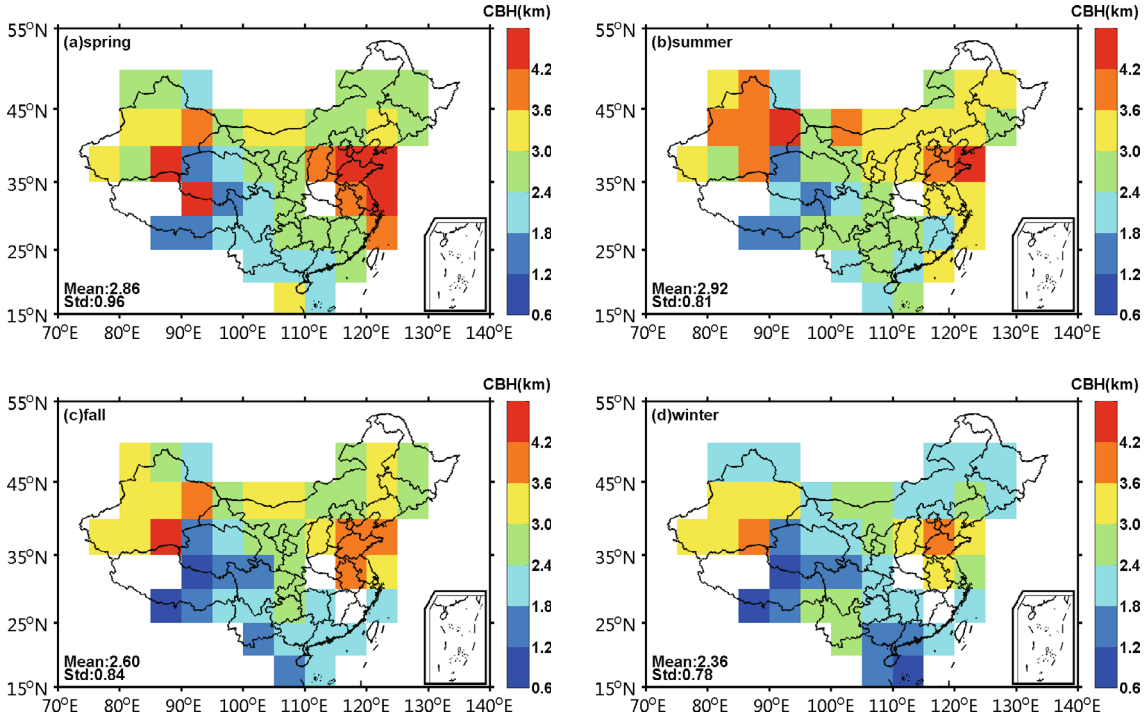


**Fig. 4.** As in Fig. 2 but for the spatial distribution of CBH at 2000 LST.

gesting cloud tends to form at low altitude. In contrast, at most sites of the YRD and NCP, about 40%–50% of cloud starts to develop at altitudes greater than 3.6 km AGL, for both the 0800 and 2000 LST observations, indicating it is difficult for cloud to form in the lower atmospheric boundary layer. Mid-level cloud (2.0 km < CBH < 3.6 km) can be frequently (about 40%–50%) observed at most sites in Xinjiang Uygur Autonomous Region (Figs. 4c–d). For almost all sites in Southeast China, less than 30% of CBHs belong to mid-level cloud, at both 0800 and 2000 LST, due to their CBHs ranging between 2.0 km and 3.6 km AGL.

To improve the forecasting accuracy of high-impact stormy weather in summer, atmospheric profile measurements at 0200 LST and 1400 LST are required at most sites of the CRN, in addition to the usual operational soundings at 0800 LST and 2000 LST. Figure 6 presents frequency histograms for the CBHs at 0200 LST, 0800 LST, 1400 LST, and 2000 LST during the period 2006–16 for all radiosonde sites in China. As also can be seen, 50% of valid CBH retrievals are less than 2.4 km AGL, which is slightly higher than 2.0 km for the CBHs at 2000 LST. On average, the frequency distribution of CBHs at 0200 LST is quite similar to that at 1400 LST. That is, about half of the CBHs are less than 1.6 km AGL.

### 3.4. *Diurnal variation of CBH*

The additional one or two soundings (i.e., 0200 LST and 1400 LST) at some sites of the CRN provide us with a unique opportunity to investigate the diurnal cycle of CBH across China from a radiosonde perspective. Figure 7 shows the spatial distributions of average CBH at 0200 LST, 0800 LST, 1400 LST and 2000 LST for the period 2006–16. Overall, the average CBH at 0200 LST and 1400 LST is slightly lower that that at 0800 LST and 2000 LST. Our understanding is that the soundings at 0200 LST and 1400 LST are mainly launched under atmospheric conditions favorable for the initiation and development of precipitation, which will inevitably lead to the more frequent occurrence of low precipitating cloud. This at least accounts for the lower CBH observed at 1400 LST despite the stronger solar-radiation induced convection in summer.

Interestingly, we can still see a distinct spatial discrepancy in the CBH at 1400 LST, which is the same as that obtained at 0800 LST and 2000 LST. For instance, most of the sites on the NCP, and in Xinjiang, are characterized by high CBH, which is generally greater than 3.0 km AGL. The lowest CBH at 1400 LST tends to occur in the PRD, which is lower than 1.2 km AGL.

As for the annual average CBH at 0800 LST, the maximum CBH tends to occur on the NCP and in the YRD, as opposed to the minimum CBH seen on the TP. In terms of the geographic distribution of the annual average CBH at 2000 LST, the contrast does not change too much.

Accounting for the large longitudinal difference (63°E) between the radiosonde sites of the CRN, the time when the CBH is calculated had to be converted to LST, which should better represent the diurnal cycle of CBH. Putting all the CBHs together, the height-resolved frequency distributions of CBH during the course of a day for the period of 2006–16 were calculated for all radiosonde sites of the CRN (Fig. 8). On the whole, a gap exists due to the scarcity of valid CBH retrievals at 0300, 0400, 1000, 1600, 2200, 2300 and 2400

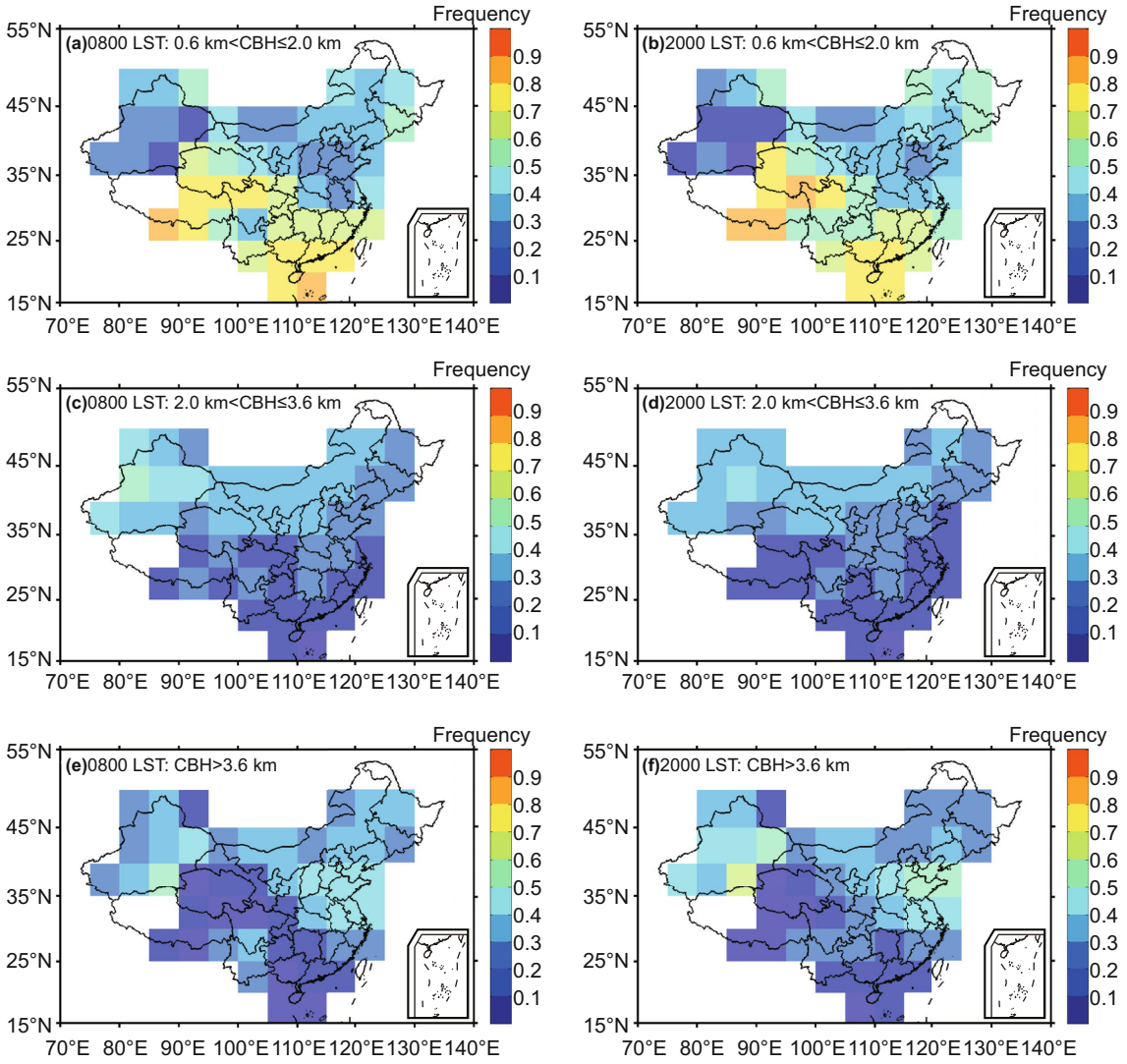


**Fig. 5.** Spatial distribution of the occurrence frequency for CBH within 0.6–2.0 km AGL at (a) 0800 LST and (b) 2000 LST, within 2.0–3.6 km AGL at (c) 0800 LST and (d) 2000 LST, and at higher than 3.6 km AGL at (e) 0800 LST and (f) 2000 LST, all of which are averaged over the period of 2006–16.

LST. In particular, more low cloud (CBH < 2.0 km) tends to form at 0100, 0800, 1400, 1900 and 2000 LST, as compared with that at other times. The frequency distribution more or less reveals the zonal distribution of the radiosonde sites of the CRN.

## 4. Concluding remarks

Taking advantage of extensive high-resolution radiosonde measurements acquired from 120 sites of the CRN during 2006–16, we produced a climatology of CBH in China by applying an RH threshold method to 421 729 individual radiosonde atmospheric profiles. The statistics regarding the CBH at diurnal and seasonal time scales across China have been presented. To the best of our knowledge, the climatology of CBH produced in this study is the first to elucidate the spatial and temporal distribution of CBH in China from a large-scale sounding perspective.

Overall, CBH does not show any distinct latitudinal dependence; rather, it exhibits large spatial variability across China, at both 0800 LST and 2000 LST, for all seasons. In particular, the highest cloud tends to occur in relatively dry regions, such as Inner Mongolia, Xinjiang, and the NCP. In contrast, the TP, YRD and SCB have relatively low CBH (< 2.4 km AGL). Meanwhile, the CBH also exhibits large seasonal variability; peak CBH is found at most sites of the CRN in summer, followed by spring and fall, with the lowest CBH observed in winter. On average, roughly 70% of cloud belongs to low cloud over the TP, YRD and SCB, due to the mean CBH being less than 2.0 km AGL. In contrast, at most sites of the YRD and NCP, about 40%–50% of cloud develops to high altitude. Interestingly, no marked diurnal cycle can be found for CBH across all sites of the CRN, most likely due to the extra soundings at 1400 LST in summertime launched for improving the numerical forecasting of high-impact weather.

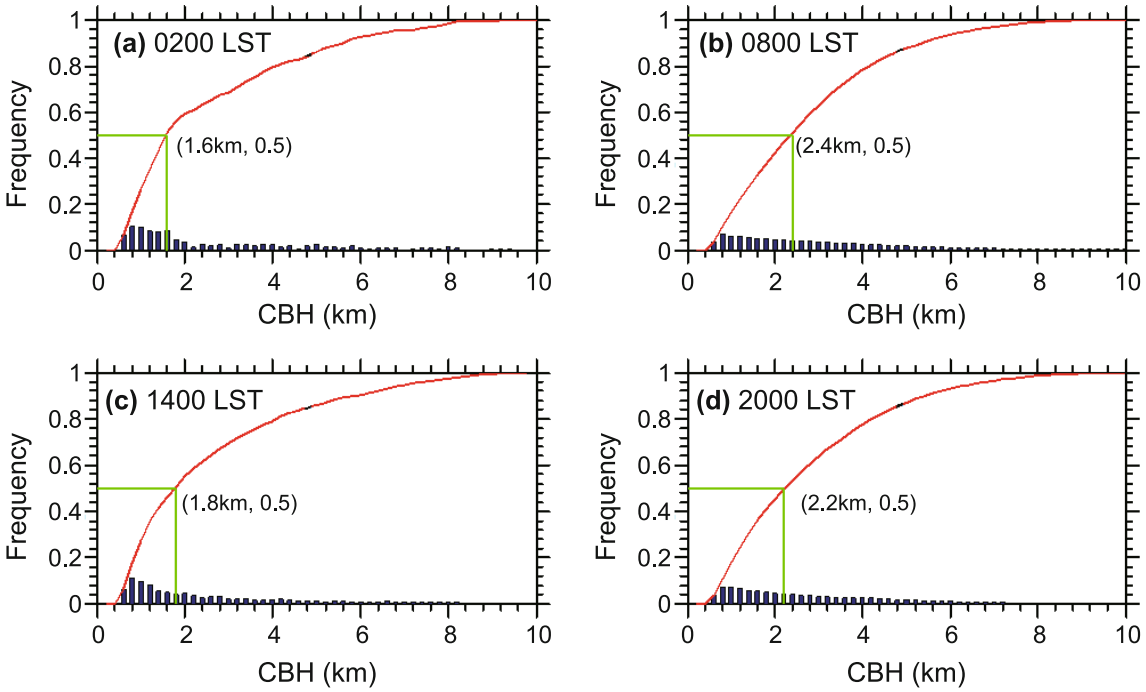


**Fig. 6.** Histogram of CBH at (a) 0200 LST, (b) 0800 LST, (c) 1400 LST, and (d) 2000 LST, during 2006–16, for all radiosonde sites in China. The red curves indicate the accumulated frequency, whereas vertical green lines indicate the frequency of 50%.

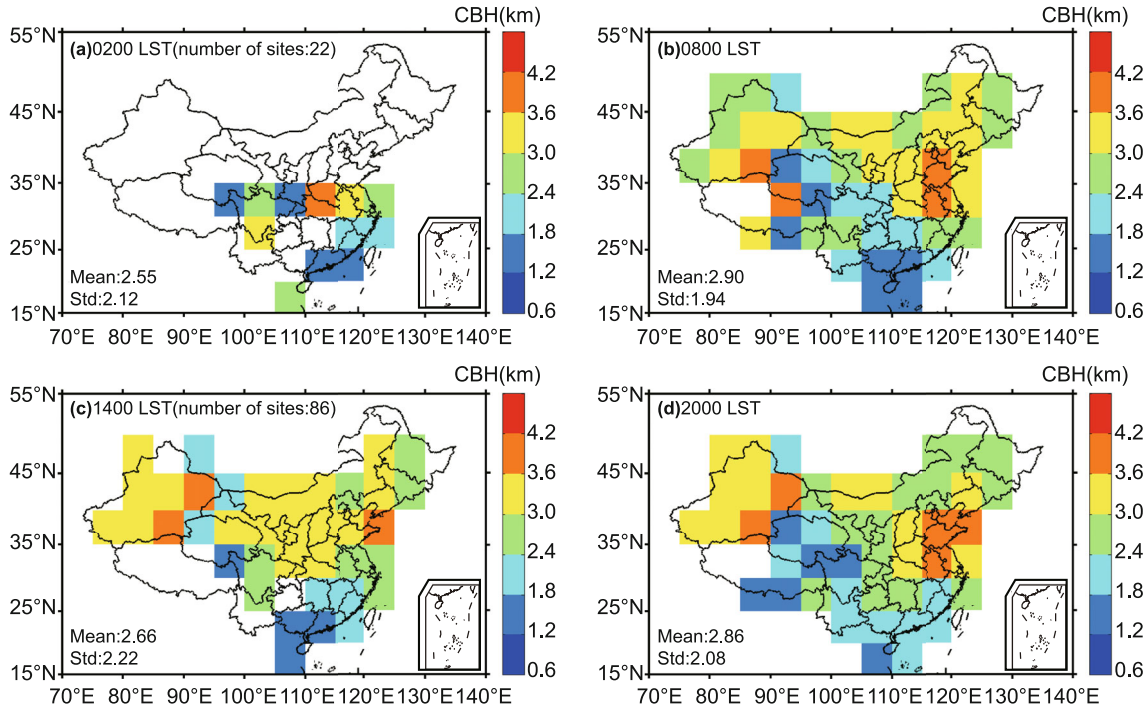


**Fig. 7.** Spatial distribution of annual-mean CBH for each 5° × 5° grid across China at (a) 0200 LST, (b) 0800 LST, (c) 1400 LST, and (d) 2000 LST, for the period 2006–16, and the mean CBH and its corresponding standard deviation (lower-left corner of each panel).

This study is just the first step in an attempt to fully understand the spatial and temporal distribution of CBH in China, which will provide a viable approach to obtain observational cloud-base information. Such information will in turn assist in better quantifying the cloud response to the increased aerosol pollution in recent years (Guo et al., 2011). However, the factors accounting for such a large spatial discrepancy have not been fully analyzed, which merits further detailed

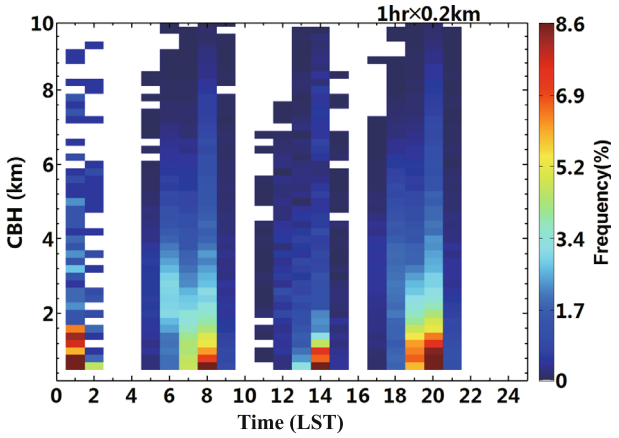


**Fig. 8.** Height-resolved frequency of CBH retrieved from all valid soundings in China during the course of a day (in LST) in summer during 2006–16.

investigation in the future. In addition, more insight should be gained into the true diurnal cycle of CBH if more routine 1400 LST sounding observations become available.

***Acknowledgements.*** This work was carried out under the auspices of the Megacities Experiment on Integrated Meteorological Observations in China initiated by the China Meteorological Administration (CMA), the Ministry of Science and Technology of China (Grant Nos. 2017YFC1501701, 2017YFC1501401, 2017YFA0603501 and 2016YFA0600403), the National Natural Science Foundation of China (Grant Nos. 91544217, 41771399 and 41471301), the Chinese Academy of Meteorological Sciences (Grant Nos. 2017Z005 and 2017R001), and the Fundamental Research Funds for the Central Universities (Grant No. 2017STUD17). The authors would like to acknowledge the CMA for providing the radiosonde data used in this study. Last but not least, we thank the anonymous reviewers for their constructive suggestions and comments, which helped improve this manuscript.

***Electronic supplementary material:*** Supplementary material is available in the online version of this article at https://doi.org/10.1007/s00376-017-7096-0.

## REFERENCES

An, N., K. C. Wang, C. L. Zhou, and R. T. Pinker, 2017: Observed variability of cloud frequency and cloud-base height within 3600 m above the surface over the contiguous United States. *J. Climate*, **30**, 3725–3742, https://doi.org/10.1175/JCLI-D-16-0559.1.

Baker, M. B., and T. Peter, 2008: Small-scale cloud processes and climate. *Nature*, **451**, 299–300, https://doi.org/10.1038/nature06594.

Bian, J. C., H. B. Chen, H. Vömel, Y. J. Duan, Y. J. Xuan, and D. R. Lü, 2011: Intercomparison of humidity and temperature sensors: GTS1, Vaisala RS80, and CFH. *Adv. Atmos. Sci.*, **28**, 139–146, https://doi.org/10.1007/s00376-010-9170-8.

Borg, L. A., R. E. Holz, and D. D. Turner, 2011: Investigating cloud radar sensitivity to optically thin cirrus using collocated Raman lidar observations. *Geophys. Res. Lett.*, **38**, L05807, https://doi.org/10.1029/2010GL046365.

Chen, T. M., J. P. Guo, Z. Q. Li, C. F. Zhao, H. Liu, M. Cribb, F. Wang, and J. He, 2016: A *CloudSat* perspective on the cloud climatology and its association with aerosol perturbations in the vertical over Eastern China. *J. Atmos. Sci.*, **73**, 3599–3616, https://doi.org/10.1175/JAS-D-15-0309.1.

Chernykh, I. V., O. A. Alduchov, and R. E. Eskridge, 2001: Trends in low and high cloud boundaries and errors in height determination of cloud boundaries. *Bull. Amer. Meteor. Soc.*, **82**, 1941–1947, https://doi.org/10.1175/1520-0477(2001)082<1941:TILAHC>2.3.CO;2.

Clement, A. C., R. Burgman, and J. R. Norris, 2009: Observational and model evidence for positive low-level cloud feedback. *Science*, **325**, 460–464, https://doi.org/10.1126/science.1171255.

Costa-Surós, M., J. Calbó, J. A. González, and J. Martin-Vide, 2013: Behavior of cloud base height from ceilometer measurements. *Atmos. Res.*, **127**, 64–76, https://doi.org/10.1016/j.atmosres.2013.02.005.

Dai, A. G., T. R. Karl, B. M. Sun, and K. E. Trenberth, 2006: Recent trends in cloudiness over the United States: A tale of monitoring inadequacies. *Bull. Amer. Meteor. Soc.*, **87**, 597–606, https://doi.org/10.1175/BAMS-87-5-597.

Davies, R., and M. Molloy, 2012: Global cloud height fluctuations measured by MISR on Terra from 2000 to 2010. *Geophys. Res. Lett.*, **39**, L03701, https://doi.org/10.1029/2011GL050506.

Dong, X.Q., B. K. Xi, and P. Minnis, 2006: A climatology of midlatitude continental clouds from the ARM SGP central facility. Part II: Cloud fraction and surface radiative forcing. *J. Climate*, **19**, 1765–1783, https://doi.org/10.1175/JCLI3710.1.

Eastman, R., and S. G. Warren, 2013: A 39-yr survey of cloud changes from land stations worldwide 1971-2009: Long-term trends, relation to aerosols, and expansion of the tropical belt. *J. Climate*, **26**, 1286–1303, https://doi.org/10.1175/JCLI-D-12-00280.1.

Eastman, R., and S. G. Warren, 2014: Diurnal cycles of cumulus, cumulonimbus, stratus, stratocumulus, and fog from surface observations over land and ocean. *J. Climate*, **27**, 2386–2404, https://doi.org/10.1175/JCLI-D-13–00352.1.

Eastman, R., S. G. Warren, and C. J. Hahn, 2011: Variations in cloud cover and cloud types over the ocean from surface observations, 1954–2008. *J. Climate*, **24**, 5914–5934, https://doi.org/10.1175/2011JCLI3972.1.

Evan, A. T., and J. R. Norris, 2012: On global changes in effective cloud height. *Geophys. Res. Lett.*, **39**, L19710, https://doi.org/10.1029/2012GL053171.

Garand, L., C. Grassotti, J. Halle, and G. Klein, 1992: On differences in radiosonde humidity-reporting practices and their implications for numerical weather prediction and remote sensing. *Bull. Amer. Meteorol. Soc.*, **73**, 1417–1423.

Guo, J.-P., X.-Y. Zhang, Y.-R. Wu, Y. Zhaxi, H.-Z. Che, B. La, W. Wang, and X.-W. Li, 2011: Spatio-temporal variation trends of satellite-based aerosol optical depth in China during 1980-2008. *Atmos. Environ.*, **45**, 6802–6811, https://doi.org/10.1016/j.atmosenv.2011.03.068.

Guo, J. P., and Coauthors, 2016a: Delaying precipitation and lightning by air pollution over the Pearl River Delta. Part I: Observational analyses. *J. Geophys. Res.*, **121**, 6472–6488, https://doi.org/10.1002/2015JD023257.

Guo, J. P., and Coauthors, 2016b: The climatology of planetary

boundary layer height in China derived from radiosonde and reanalysis data. *Atmos. Chem. Phys.*, **16**, 13 309–13 319, https://doi.org/10.5194/acp-16-13309-2016.

Guo, J. P., and Coauthors, 2017: Declining frequency of summertime local-scale precipitation over eastern China from 1970 to 2010 and its potential link to aerosols. *Geophys. Res. Lett.*, **44**, 5700–5708, https://doi.org/10.1002/2017GL073533.

IPCC, 2013: *Climate Change* 2013 : *The Physical Science Basis. Contribution of Working Group I to the Fifth Assessment Report of the Intergovernmental Panel on Climate Change*, T. F. Stocker et al., Eds., Cambridge University Press, Cambridge, United Kingdom and New York, NY, USA, 1535 pp, https://doi.org/10.1017/CBO9781107415324.

Kato, S., and Coauthors, 2011: Improvements of top-of-atmosphere and surface irradiance computations with CALIPSO-, CloudSat-, and MODIS-derived cloud and aerosol properties. *J. Geophys. Res.*, **116**, D19209, https://doi.org/10.1029/2011JD016050.

Kiehl, J. T., and K. E. Trenberth, 1997: Earth's annual global mean energy budget. *Bull. Amer. Meteor. Soc.*, **78**, 197–208, https://doi.org/10.1175/1520-0477(1997)078<0197:EAGMEB>2.0.CO;2.

Klein, S. A., and D. L. Hartmann, 1993: The seasonal cycle of low stratiform clouds. *J. Climate*, **6**, 1587–1606, https://doi.org/10.1175/1520-0442(1993)006<1587:TSCOLS>2.0.CO;2.

Li, Z. Q., and Coauthors, 2016: Aerosol and Monsoon Climate Interactions over Asia. *Rev. Geophys.*, **54**, 866–929, https://doi.org/10.1002/2015RG000500.

Marchand, R., G. G. Mace, T. Ackerman, and G. Stephens, 2008: Hydrometeor detection using *Cloudsat*-an earth-orbiting 94-GHz cloud radar. *J. Atmos. Oceanic Technol.*, **25**, 519–533, https://doi.org/10.1175/2007JTECHA1006.1.

Martucci, G., C. Milroy, and C. D. O'Dowd, 2010: Detection of cloud-base height using Jenoptik CHM15K and Vaisala CL31 ceilometers. *J. Atmos. Oceanic Technol.*, **27**, 305–318, https://doi.org/10.1175/2009JTECHA1326.1.

Miao, Y. C., J. P. Guo, S. H. Liu, H. Liu, Z. Q. Li, W. C. Zhang, and P. M. Zhai, 2017: Classification of summertime synoptic patterns in Beijing and their association with boundary layer structure and aerosol pollution. *Atmos. Chem. Phys.*, **17**, 3097–3110, https://doi.org/10.5194/acp-17-3097-2017.

Minnis, P., and E. F. Harrison, 1984: Diurnal variability of regional cloud and clear-sky radiative parameters derived from GOES data. Part I: Analysis method. *J. Climate Appl. Meteor.*, **23**, 993–1011, https://doi.org/10.1175/1520-0450(1984)023<0993:DVORCA>2.0.CO;2.

Morel, C., and S. Senesi, 2002: A climatology of mesoscale convective systems over Europe using satellite infrared imagery. I: Methodology. *Quart. J. Roy. Meteor. Soc.*, **128**, 1953–1971, https://doi.org/10.1256/003590002320603485.

Myers, T. A., and J. R. Norris, 2015: On the relationships between subtropical clouds and meteorology in observations and CMIP3 and CMIP5 models. *J. Climate*, **28**, 2945–2967, https://doi.org/10.1175/JCLI-D-14-00475.1.

Naud, C. M., A. D. D. Genio, M. Bauer, and W. Kovari, 2010: Cloud vertical distribution across warm and cold fronts in *CloudSat*-CALIPSO data and a General Circulation Model. *J. Climate*, **23**, 3397–3415, https://doi.org/10.1175/2010JCLI3282.1.

Poore, K. D., J. H. Wang, and W. B. Rossow, 1995: Cloud layer thicknesses from a combination of surface and upper-air observations. *J. Climate*, **8**, 550–568, https://doi.org/10.1175/1520-0442(1995)008<0550:CLTFAC>2.0.CO;2.

Sassen, K., and Z. E. Wang, 2008: Classifying clouds around the globe with the CloudSat radar: 1-year of results. *Geophys. Res. Lett.*, **35**, L04805, https://doi.org/10.1029/2007GL032591.

Sharma, S., R. Vaishnav, M. V. Shukla, P. Kumar, P. Kumar, P. K. Thapliyal, S. Lal, and Y. B. Acharya, 2016: Evaluation of cloud base height measurements from Ceilometer CL31 and MODIS satellite over Ahmedabad, India. *Atmospheric Measurement Techniques*, **9**, 711–719, https://doi.org/10.5194/amt-9-711-2016.

Shonk, J. K. P., R. J. Hogan, and J. Manners, 2012: Impact of improved representation of horizontal and vertical cloud structure in a climate model. *Climate Dyn.*, **38**, 2365–2376, https://doi.org/10.1007/s00382-011-1174-2.

Stephens, G. L., 2005: Cloud feedbacks in the climate system: A critical review. *J. Climate*, **18**, 237–273, https://doi.org/10.1175/JCLI-3243.1.

Stephens, G. L., and Coauthors, 2002: The CloudSat Mission and the A-Train: A new dimension of space-based observations of clouds and precipitation. *Bull. Amer. Meteor. Soc.*, **83**, 1771–1790, https://doi.org/10.1175/BAMS-83-12-1771.

Stephens, G. L., and Coauthors, 2012: An update on Earth's energy balance in light of the latest global observations. *Nature Geoscience*, **5**, 691–696, https://doi.org/10.1038/ngeo1580.

Sun, B. M., T. R. Karl, and D. J. Seidel, 2007: Changes in cloud-ceiling heights and frequencies over the United States since the early 1950s. *J. Climate*, **20**, 3956–3970, https://doi.org/10.1175/JCLI4213.1.

Wang, F., and Coauthors, 2015: Multi-sensor quantification of aerosol-induced variability in warm cloud properties over eastern China. *Atmos. Environ.*, **113**, 1–9, https://doi.org/10.1016/j.atmosenv.2015.04.063.

Wang, J. H., and W. B. Rossow, 1995: Determination of cloud vertical structure from upper-air observations. *J. Appl. Meteor.*, **34**, 2243–2258, https://doi.org/10.1175/1520-0450(1995)034<2243:DOCVSF>2.0.CO;2.

Warren, S. G., R. M. Eastman, and C. J. Hahn, 2007: A survey of changes in cloud cover and cloud types over land from surface observations, 1971–96. *J. Climate*, **20**, 717–738, https://doi.org/10.1175/JCLI4031.1.

Warren, S. G., C. J. Hahn, J. London, R. M. Chervin, and R. L. Jenne, 1986: Global distribution of total cloud cover and cloud type amounts over land. NCAR Technical Note NCAR/TN-273+STR, National Center for Atmospheric Research, Boulder, CO, 29 pp, https://doi.org/10.5065/D6GH9FXB.

Warren, S. G., C. J. Hahn, J. London, R. M. Chervin, and R. L. Jenne, 1988: Global distribution of total cloud cover and cloud type amounts over the ocean. NCAR Technical Note NCAR/TN-317+STR, National Center for Atmospheric Research, Boulder, CO, 42 pp, https://doi.org/10.5065/D6QC01D1.

Wild, M., 2012: New Directions: A facelift for the picture of the global energy balance. *Atmos. Environ.*, **55**, 366–367, https://doi.org/10.1016/j.atmosenv.2012.03.022.

Zelinka, M. D., S. A. Klein, K. E. Taylor, T. Andrews, M. J. Webb, J. M. Gregory, and P. M. Forster, 2013: Contributions of different cloud types to feedbacks and rapid adjustments in CMIP5. *J. Climate*, **26**, 5007–5027, https://doi.org/10.1175/JCLI-D-12-00555.1.

Zhang, J. Q., H. B. Chen, Z. Q. Li, X. H. Fan, L. Peng, Y. Yu, and M. Cribb, 2010: Analysis of cloud layer structure in

Shouxian, China using RS92 radiosonde aided by 95 GHz cloud radar. *J*. *Geophys*. *Res*., **115**, D00K30, https://doi.org/10.1029/2010JD014030.

Zhang, J. Q., X. A. Xia, and H. B. Chen, 2017a: A comparison of cloud layers from ground and satellite active remote sensing at the Southern Great Plains ARM site. *Adv*. *Atmos*. *Sci*., **34**, 347–359, https://doi.org/10.1007/s00376-016-6030-1.

Zhang, L., X. Q. Dong, A. Kennedy, B. K. Xi, and Z. Q. Li, 2017b: Evaluation of NASA GISS post-CMIP5 single column model simulated clouds and precipitation using ARM Southern Great Plains observations. *Adv*. *Atmos*. *Sci*., **34**, 306–320, https://doi.org/10.1007/s00376-016-5254-4.

Zhou, C., M. D. Zelinka, and S. A. Klein, 2016: Impact of decadal cloud variations on the Earth's energy budget. *Nature Geoscience*, **9**, 871–874, https://doi.org/10.1038/NGEO2828.